Thin Solid Films 520 (2012) 2966–2970

Contents lists available at SciVerse ScienceDirect

Thin Solid Films

journal homepage: www.elsevier.com/locate/tsf

All fluorescent and high color rendering index white organic light-emitting devices with improved color stability at high brightness

Shiming Zhang [a], Guohua Xie [a], Qin Xue [b], Zhensong Zhang [a], Li Zhao [a], Yang Luo [a], Shouzhen Yue [a], Yi Zhao [a,*], Shiyong Liu [a]

[a] State Key laboratory on Integrated Optoelectronics, College of Electronic Science and Engineering, Jilin University, Changchun 130012, People's Republic of China
[b] College of Physical Science and Technology, Central China Normal University, Wuhan 430079, People's Republic of China

ARTICLE INFO

Article history:
Received 17 April 2011
Received in revised form 18 October 2011
Accepted 21 October 2011
Available online 29 October 2011

Keywords:
Fluorescent emitters
White organic light-emitting diodes
Color rendering index
Trapping
Energy transfer

ABSTRACT

We have demonstrated high color rendering index (CRI) white organic light-emitting devices using a multilayer structure based on all fluorescent emitters. The CRI of white light can be easily tuned by adjusting the thickness of the blue emitting layer (B-EML). In particular, the device with 8-nm-thick B-EML obtains very high CRI values (91–92) over a wide range of luminance (4000–23,000 cd/m^2). Furthermore, the Commission Internationale De L'Eclairage coordinates of the device is rather stable and the variation is only ($\pm$0.005, $\pm$0.003) over 4000–23,000 cd/m^2. The values are very close to white light equivalent energy point of (0.333, 0.333). We attribute these unique performances to the competition of the two mechanisms of the carrier trapping of the red dopant and efficient förster energy transfer in the blue emitting layer.

1. Introduction

Since the reports of white-emitting devices by the group of Kido [1,2], white organic light-emitting devices (WOLEDs) have attracted considerable attention due to their potential applications in flat panel displays [3–7]. OLEDs possess many advantages such as ultra-thin, light weight, and environmental friendliness. As a result, OLEDs are considered as one of the candidates for next generation planar lighting source [5]. Though WOLEDs with a power efficiency of 90 lm/W have already approached the fluorescent lamps [4], it still requires further improvement in many aspects: e.g. simplifying the device structure, increasing the stability of Commission Internationale De L'Eclairage (CIE) chromaticity coordinates, and improving the color rendering index (CRI). To date, several methods have been reported to prepare high CRI and color-stable devices [8–12]. In order to achieve high CRI, red–green–blue (RGB) elements are essential. However, it is very difficult to attain balanced white emission under different bias conditions. Consequently, electroluminescence (EL) is often changed with increased voltage, especially if more than one dopant is used [13]. In recent years, phosphorescent materials are widely used due to the potential for achieving 100% internal quantum efficiency [14]. However, compared with fluorescent WOLEDs, phosphorescent WOLEDs typically have shorter operational lifetime [6]. Basically, the shorter operational lifetime of blue phosphors worsens the color stability of all-phosphorescent WOLEDs, especially at high brightness. This is a challenge for applications such as passive matrix-driven displays, high brightness displays, or OLEDs for high brightness lighting applications where the development of OLEDs has lagged behind that of light-emitting diodes (LEDs) [15,16]. Therefore, further studies on preparation of all fluorescent devices to provide more stable WOLEDs with excellent performances at high brightness are very important.

In this paper, we demonstrate high CRI WOLEDs with improved color stability at high brightness using all fluorescent architecture. The CRI of WOLEDs can be easily adjusted. Three emissive dopant materials (4-(Dicyanomethylene)-2-tert-butyl-6-(1,1,7,7-tetramethyljulolidin-4-yl-vinyl)-4H-pyran (DCJTB), 2,3,6,7-Tetrahydro-1,1,7,7,-tetramethyl-1H,5H,11H-10-(2-benzothiazo lyl) quinolizino-[9, 9a, 1gh] comarin (C545T), and 4,4′-Bis(9-ethyl-3-carbazovinylene)-1, 1′-biphenyl (BCzVBi)) were employed to emit R, G, and B colors, respectively, and whose molecule structures were demonstrated in Fig. 1. In the triple-emission-layer system, the charge-carrier trapping sites formed on DCJTB molecules and efficient host–guest energy transfer from 4,40-bis(2,2-diphenylvinyl)-1,10-biphenyl (DPVBi) to BCzVBi could lead to a balanced exciton distribution across the emission region. The WOLEDs exhibit high CRI values and fairly stable CIE coordinates at high brightness.

2. Experimental details

The WOLED is based on the blue emitter BCzVBi and the red emitter DCJTB doped into a common host material DPVBi and the green emitter C545T doped into tris(8-hydroxy-quinolinato) aluminium

* Corresponding author. Tel.: +86 431 85168242 8301.
E-mail address: zhao_yi@jlu.edu.cn (Y. Zhao).

0040-6090/$ – see front matter © 2011 Elsevier B.V. All rights reserved.
doi:10.1016/j.tsf.2011.10.148

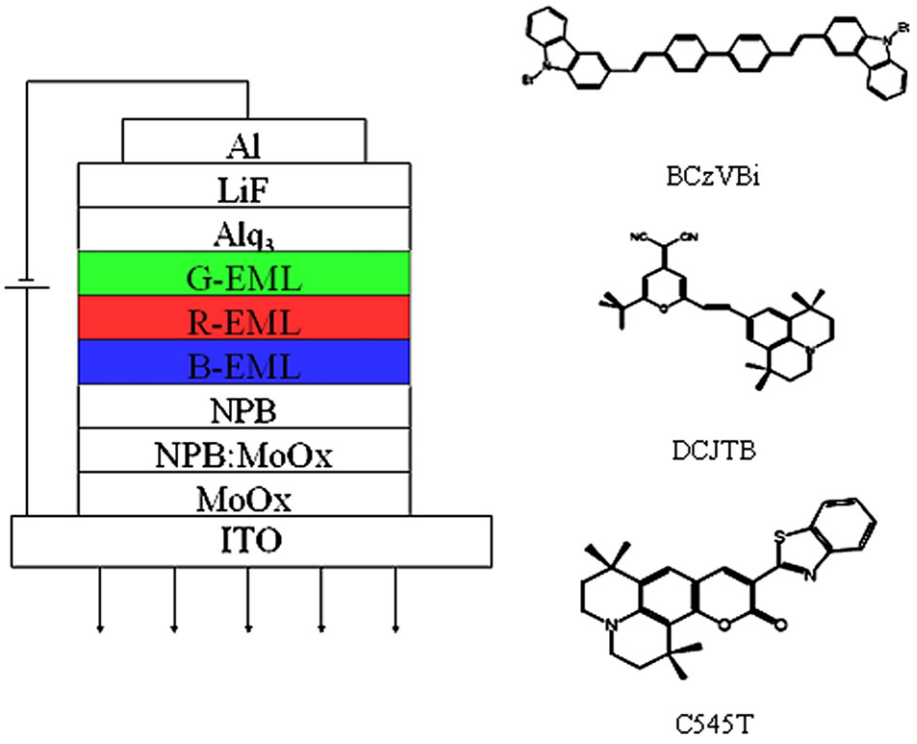

Fig. 1. Schematic configuration of WOLEDs and chemical structures of emissive materials used in this paper.

(Alq_3) respectively. Prior to the device fabrication, indium tin oxide (ITO)-coated glass substrates were carefully cleaned by scrubbing and sonication. All the devices were fabricated with the conventional process. N,N′-Bis(naphthalen-1-yl)-N,N′-bis(phenyl)-benzidine (NPB) and Alq_3, serve as hole-transporting layer and electron transporting layer (ETL), respectively. The MoO_x buffer layer is thermally deposited onto ITO substrate, following with NPB: MoO_x p-doping layer to reduce the ohmic loss [17]. The device structures were ITO/MoO_x(2 nm)/NPB:MoO_x(15 wt.%, 10 nm)/NPB(40 nm)/DPVBi:BCzVBi(5 wt.%, *x* nm)/DPVBi:DCJTB(1 wt.%, 10 nm)/Alq_3:C545T (1 wt.%, 10 nm)/Alq_3 (30 nm)/LiF(1 nm)/Al, as shown in Fig. 1. The thermal deposition rates were 0.1, 0.05, and 0.5 nm/s for organic materials, LiF, and Al, respectively. The active area of the devices was 4 mm^2. The EL spectra and CIE coordinates of the devices were measured by a PR650 spectroscan spectrometer, and the current (J)–voltage (V)–luminance (L) characteristics were recorded simultaneously by combining the spectrometer with Keithley 2400 programmable voltage–current source. The CRI values of the devices were calculated with software SETFOS 3.0 from FLUXIM AG. All measurements were carried out at room temperature under ambient conditions.

3. Results and discussions

We fabricated devices with the structure of ITO/MoO_x(2 nm)/NPB:MoO_x(15 wt.%, 10 nm)/NPB(40 nm)/DPVBi:BCzVBi(5 wt.%, *x* nm)/DPVBi:DCJTB(1 wt.%, 10 nm)/Alq_3:C545T (1 wt.%, 10 nm)/Alq_3 (30 nm)/LiF(1 nm)/Al, $x = 10$, 8, 6 nm for devices A, B and C, respectively. Fig. 2 shows the normalized EL spectra of the devices A, B and C at the voltage of 8 V. The devices exhibit four-peak EL spectra: two emission peaks at about 444 and 472 nm are due to BCzVBi, while 520 and 588 nm peaks from C545T and DCJTB, respectively. As can be seen, the emission intensity of BCzVBi increases with the thickness of blue emitting layer (B-EML) varying from 6 to10 nm. The increase in emission intensity of BCzVBi could be easily interpreted by more excitons formation in the B-EML with increasing thickness. In addition, increase in B-EML thickness can also broaden the recombination zone that results in reducing exciton quenching, contributing to the enhancements of emission in the B-EML.

The normalized EL spectra of WOLEDs at different voltages are shown in Fig. 3. It can be seen that a significantly broader EL spectrum ranging from 400 to 700 nm, which completely covers the total wavelength region of visible light, was obtained. A relatively larger increase in blue with respect to the red emission (ratio of the photons from BCzVBi and DCJTB emission: $R_{blue/red}$) was found in EL spectra at low voltages (<7 V). However, it is noteworthy that the $R_{blue/red}$ value is nearly unchanged at high voltages (7–10 V). The characteristic of the EL spectra at high voltages indicates balanced emission across the RGB EMLs. We attribute this phenomenon to the competition of the two mechanisms of carrier trapping of the red dopant and förster energy transfer in the B-EML. As is known, holes are normally major carriers compared with electrons within an OLED. In addition, the hole mobility of BCzVBi was determined to be as large as 10^{-3} cm^2 V^{-1} S^{-1}[18]. Thus, the distribution of electrons in the EML would play a key role in affecting the EL spectra of the device. According to the energy level diagram shown in Fig. 4, the HOMO (highest occupied molecular orbital) and the LUMO (lowest unoccupied molecular orbital) levels of DPVBi are 5.9 and 2.8 eV [19],

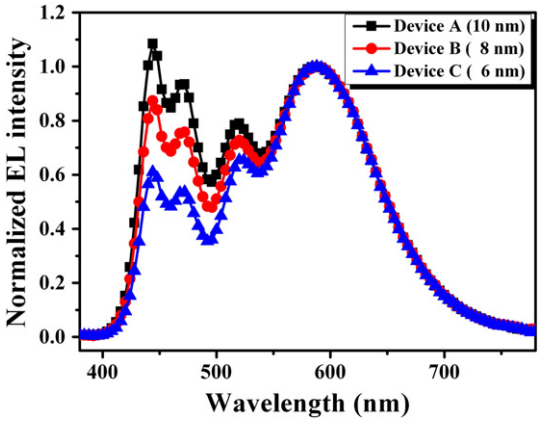

Fig. 2. Normalized spectra of the devices A, B and C at 8 V.

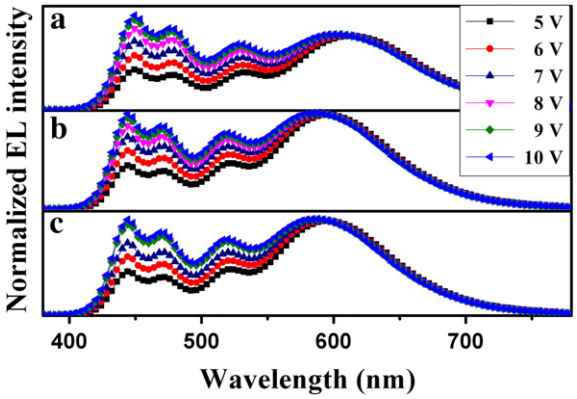

Fig. 3. Normalized EL intensity at different voltages (5–10 V) of (a) device A ,(b) device B and (c) device C, respectively.

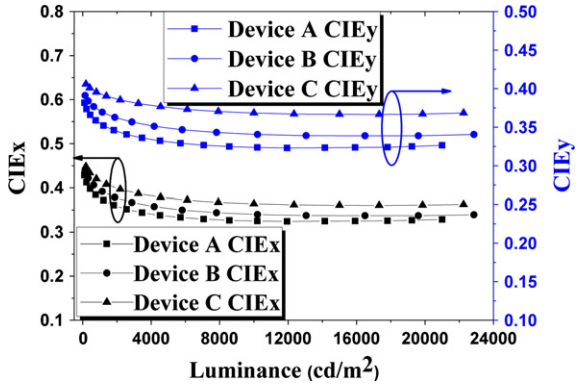

Fig. 5. CIE coordinates of devices at different luminance.

respectively, and those of DCJTB are 5.3 and 3.1 eV [20], respectively. The LUMO–LUMO offset (0.3 eV) between DCJTB and DPVBi indicates the possibility of electron trapping on DCJTB sites and the trapped electrons will subsequently recombine with holes to form excitons. Hence, at low voltages, few injected electrons could travel far enough to reach the B-EML due to the electron trapping on DCJTB molecules, which will result in a red dominating EL spectrum. However, as reported, the trapping effect of the dopant will be decreased with increasing internal electric field [21,22]. Thus, when the voltage is further increased (>7 V), more electrons could travel through the R-EML and a higher electron concentration will be obtained in the B-EML. As shown in Fig. 4, the LUMO and HOMO levels of the host material DPVBi are both lower than those of hole-transporting material NPB (HOMO, −5.2 eV; LUMO, −2.2 eV) [23]. These demonstrate that both holes and electrons can be accumulated at the NPB/B-EML interface due to the LUMO–LUMO offset (0.6 eV) and HOMO–HOMO offset (0.7 eV) between these two layers. The accumulated carriers at the interface can form adequate excitons on DPVBi molecules, and subsequently transfer singlet energy to the blue dopant BCzVBi via förster energy transfer process, leading to efficient blue emission. Hence, at high applied voltages (7–10 V), förster energy transfer from DPVBi to BCzVBi, which is independent of the internal electric field [24], will gradually play a more prominent role in influencing the EL spectrum than the trapping effect of DCJTB. As discussed above, the competition of the two mechanisms finally realizes not only efficient R and B emission but also balanced exciton distribution in the EMLs. Consequently, as shown in Fig. 5, stable CIE coordinates over a wide range of luminance is obtained.

In order to further investigate the relationship between the shift of CIE and doping concentration of DCJTB, another set of devices was fabricated and measured by fixing the B-EML at 8 nm and varying DCJTB doping concentrations to 0%, 0.5% and 2%. The inset of Fig. 6 shows the CIE coordinates of devices at different luminance of devices (including device B). We can clearly see that a much more serious CIE variation with increasing luminance was observed while we further increased the doping concentration to 2 wt.%. The result proves that the CIE variation under low luminance is because the electron trapping effect of DCJTB. As we mentioned above, holes are adequate in the EMLs. Hence, the main reason for this is the distribution of electrons in the EML. When increasing the DCJTB doping concentration, the number of electron trapping sites increases, which will cause more electrons to be trapped by DCJTB molecules at lower voltage, thus resulting in stronger DCJTB emission. In addition, higher voltage is needed for the injected electrons to reach the B-EML due to the increase in the number of electron trapping sites, leading to a more obvious CIE variation eventually. The voltage–current density (V–J) curves of the devices are also shown in Fig. 6, and as can be seen, the current density decreases with increasing DCJTB doping concentration at a fixed voltage, which is partly because of the electron trapping effect of DCJTB.

The CRI and correlated color temperature (CCT) values of WOLEDs at different voltages are shown in Fig. 7. It is clear that, besides fairly stable CIE coordinates, the WOLEDs also exhibit high CRI and ideal CCT values (2500–6500 K [25]) at high brightness. Device A reaches a maximum CRI of 93 at 7 V. Device B obtains high CRI value (91–92) when working over a wide range of luminance (4000–23,000 cd/m^2), and at the same time the CIE coordinates are (0.344 ± 0.005, 0.343 ± 0.003). The high CRI, ideal CCT and stable CIE coordinate properties of device B is comparable to or even better than some of the high-performance all fluorescent WOLEDs reported as so far [9,11,20,26]. The inset of Fig. 7 shows the CIE coordinates of the emission color of device B as a function of the viewing angle. The shifts in CIE x and y coordinates from the viewing angles of 0° to 75° are 0.0126 and 0.071, respectively. This is not expected to be a problem in display applications. We can also see

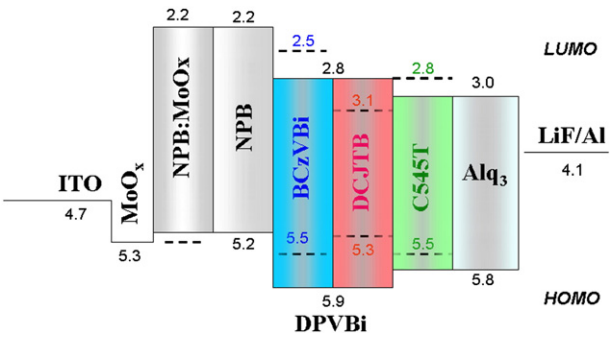

Fig. 4. The energy level diagram of devices.

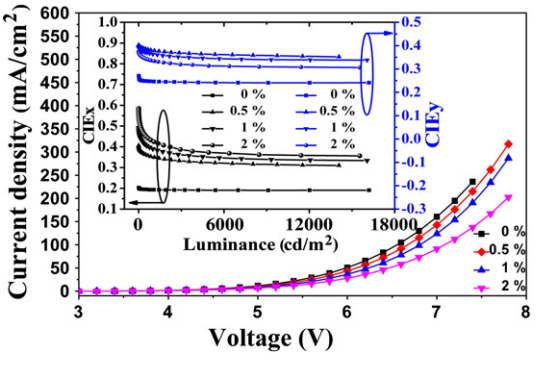

Fig. 6. Luminance–CIE coordinates (inset) and voltage–current density (V–J) characteristics of the devices with different doping concentrations of DCJTB.

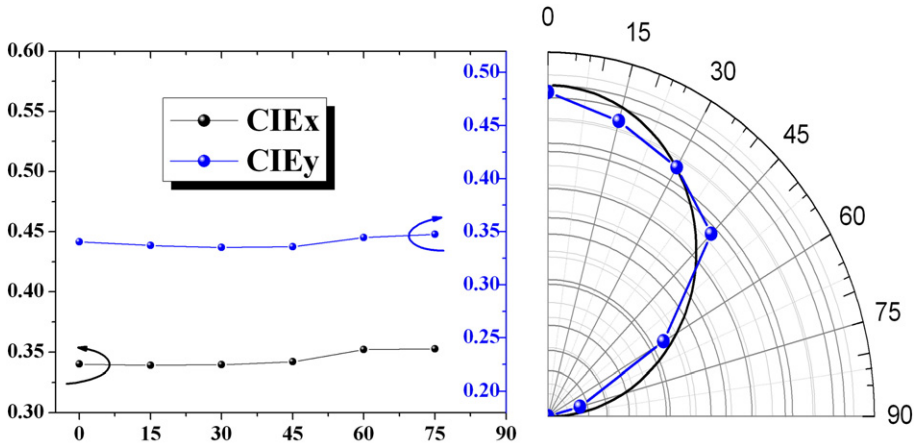

CRI/CCT (K)	5 V	6 V	7 V	8 V	9 V	10 V
Device A	81/3244	89/3800	93/4427	92/5028	90/5489	89/5734
Device B	78/3097	86/3560	91/4022	92/4413	92/4701	91/4871
Device C	76/3007	85/3410	87/3808	89/4107	89/4303	89/4354

Fig. 7. CRI and CCT values at different applied voltages of WOLEDs. The upper left-hand inset shows the CIE coordinates of device B as a function of the viewing angle. The upper right-hand inset indicates the measured angular distribution of device B and the black solid line represents a Lambertian-type distribution.

from the other inset of Fig. 7 that the emissive profiles of the device are approximately the same as the Lambertian emitter's.

Fig. 8 shows luminance as a function of the voltage and the inset shows the forward-viewing efficiency versus luminance characteristics of WOLEDs. The external quantum efficiency of the devices is calculated utilizing the method presented by Okamoto et al. [27]. We can see that device B has maximum current efficiency and brightness of 6.78 cd/A and 22860 cd/m^2, respectively. The efficiency is not very high, as the WOLED is based on all fluorescent materials and the efficiency is measured in forward direction. However, when the WOLEDs are used for solid-state lighting, the light emitted from all sections of the substrate can, in principle, be redirected to the forward direction via certain lighting fixtures applied to the forward-viewing efficiencies by a factor of 1.7–2.3 [5,28,29]. Therefore, the highest current efficiency of device B can reach 11.52–15.59 cd/A. Moreover, the performance of the devices can be further improved by replacing the Alq_3 ETL layer with an n-doped layer to form a p–i–n structure [30] and using a periodic outcoupling structure [4] to increase the light extraction. We hope more efficient WOLEDs can be developed based on this device architecture.

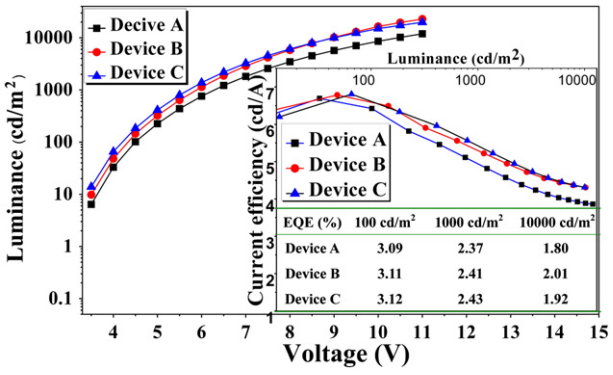

Fig. 8. Voltage–luminance curves of the WOLEDs. The inset shows the current efficiency and external quantum efficiency at different brightness of devices.

4. Conclusions

In summary, we have demonstrated WOLEDs using a multilayer structure based on all fluorescent emitting layers. The devices can take advantage of the charge-carrier trapping and efficient energy transfer to produce high CRI as well as stable CIE coordinates when working over a wide range of luminance. Moreover, the CRI of the WOLEDs can be tuned by just adjusting one emitting layer. Device B obtains high CRI value (91–92) when working over a large range of luminance (4000–23,000 cd/m^2), while device A reaches a maximum CRI as high as 93. Furthermore, the CIE coordinates of the two devices are both rather stable and very close to white light equivalent energy point of (0.333, 0.333) when working under high brightness conditions. We hope this study will be useful for the development of high CRI and color-stable WOLEDs at high brightness.

Acknowledgments

We acknowledge funding for this research from the National Basic Research Program of China (973 Program) under Grant No. 2010CB327701 and the National Natural Science Foundation of China (Grant No.60977024 and 60906021).

References

[1] J. Kido, K. Hongawa, K. Okuyama, K. Nagai, Appl. Phys. Lett. 64 (1994) 815.
[2] J. Kido, M. Kimura, K. Nagai, Science 267 (1995) 1332.
[3] Q. Xue, G.H. Xie, P. Chen, J.H. Lu, D.D. Zhang, Y.N. Tang, Y. Zhao, J.Y. Hou, S.Y. Liu, Synth. Met. 160 (2010) 829.
[4] S. Reineke, F. Lindner, G. Schwartz, N. Seidler, K. Walzer, B. Lussem, K. Leo, Nature 459 (2009) 234.
[5] B. D'Andrade, S. Forrest, Adv. Mater. 16 (2004) 1585.
[6] G. Schwartz, M. Pfeiffer, S. Reineke, K. Walzer, K. Leo, Adv. Mater. 19 (2007) 3672.
[7] S. Liu, J. Huang, Z. Xie, Y. Wang, B. Chen, Thin Solid Films 363 (2000) 294.
[8] S.H. Kim, Y. Jin, J.Y. Yu, J. Kim, S. Song, H. Suh, K. Lee, Synth. Met. 160 (2010) 835.
[9] J.H. Jou, C.J. Wang, Y.P. Lin, Y.C. Chung, P.H. Chiang, M.H. Wu, C.P. Wang, C.L. Lai, C. Chang, Appl. Phys. Lett. 92 (2008) 223504.
[10] J.Z. Zhu, W.L. Li, L.L. Han, B. Chu, G. Zhang, D.F. Yang, Y.R. Chen, Z.S. Su, J.B. Wang, S.H. Wu, T.J. Tsuboi, Opt. Lett. 34 (2009) 2946.
[11] Z.Q. Zhang, Q. Wang, Y.F. Dai, Y.P. Liu, L.X. Wang, D.G. Ma, Org. Electron. 10 (2009) 491.

[12] Y.W. Ko, C.-H. Chung, J.H. Lee, Y.-H. Kim, C.-Y. Sohn, B.-C. Kim, C.-S. Hwang, Y.-H. Song, J. Lim, Y.J. Ahn, G.-W. Kang, N. Lee, C. Lee, Thin Solid Films 426 (2003) 246.
[13] K.T. Kamtekar, A.P. Monkman, M.R. Bryce, Adv. Mater. 22 (2010) 572.
[14] C. Adachi, M.a. Baldo, M.E. Thompson, S.R. Forrest, J. Appl. Phys. 90 (2001) 5048.
[15] C.J. Humphreys, MRS Bull. 33 (2008) 459.
[16] M.R. Krames, O.B. Shchekin, R. Mueller-Mach, G.O. Mueller, L. Zhou, G. Harbers, M.G. Craford, J. Disp. Technol. 3 (2007) 160.
[17] G.H. Xie, Y.L. Meng, F.M. Wu, C. Tao, D.D. Zhang, M.J. Liu, Q. Xue, W. Chen, Y. Zhao, Appl. Phys. Lett. 92 (2008) 093305.
[18] C. Hosokawa, H. Tokailin, H. Higashi, T. Kusumoto, Appl. Phys. Lett. 63 (1993) 1322.
[19] P. Chen, Q. Xue, W.F. Xie, Y. Duan, G.H. Xie, Y. Zhao, J.Y. Hou, S.Y. Liu, L.Y. Zhang, B. Li, Appl. Phys. Lett. 93 (2008) 153508.
[20] H.P. Lin, D.B. Yu, X.W. Zhang, J. Li, L.A. Zhang, X.Y. Jiang, Z.L. Zhang, Semicond. Sci. Technol. 25 (2010) 105004.
[21] Q. Wang, J. Ding, D. Ma, Y. Cheng, L. Wang, X. Jing, F. Wang, Adv. Funct. Mater. 19 (2009) 84.
[22] M.C. Gather, R. Alle, H. Becker, K. Meerholz, Adv. Mater. 19 (2007) 4460.
[23] X. Xu, S. Chen, G. Yu, C. Di, H. You, D. Ma, Y. Liu, Adv. Mater. 19 (2007) 1281.
[24] A.R. Clapp, I.L. Medintz, H. Mattoussi, Chem. Phys. Chem. 7 (2006) 47.
[25] M.C. Gather, A. Köhnen, K. Meerholz, Adv. Mater. 23 (2011) 233.
[26] Y.-C. Tsai, J.-H. Jou, Appl. Phys. Lett. 89 (2006) 243521.
[27] S. Okamoto, K. Tanaka, Y. Izumi, H. Adachi, T. Yamaji, T. Suzuki, Jpn. J. Appl. Phys. Part 2 Lett. 40 (2001) L783.
[28] B.W. D'Andrade, R.J. Holmes, S.R. Forrest, Adv. Mater. 16 (2004) 624.
[29] X. Gong, S. Wang, D. Moses, G.C. Bazan, A.J. Heeger, Adv. Mater. 17 (2005) 2053.
[30] G. He, M. Pfeiffer, K. Leo, M. Hofmann, J. Birnstock, R. Pudzich, J. Salbeck, Appl. Phys. Lett. 85 (2004) 3911.